Collisional-radiative model for an argon glow discharge

Annemie Bogaerts[a] and Renaat Gijbels
Department of Chemistry, University of Antwerp, Universiteitsplein 1, B-2610 Wilrijk-Antwerp, Belgium

Jaroslav Vlcek
Department of Physics, University of West Bohemia, P.O. Box 314, 306 14 Plzen, Czech Republic

(Received 17 September 1997; accepted for publication 8 April 1998)

An extensive collisional-radiative model for the argon atoms in a glow discharge has been developed. Sixty-five effective argon atomic levels are considered. The processes taken into account are radiative decay, electron, fast argon ion and argon atom and thermal argon atom impact ionization, excitation and deexcitation between all the levels, electron-ion radiative recombination, and electron-ion three-body recombination where the third body is an electron, fast argon ion or atom, or a thermal argon atom. Some additional processes are incorporated for the two 4*s* metastable levels, i.e., Penning ionization of sputtered atoms, two- and three-body collisions with argon ground state atoms, collisions between two atoms in a metastable level, and diffusion and subsequent deexcitation at the walls. Typical results of the model are the populations of the various excited levels as a function of distance, and the relative contributions of different populating and depopulating processes for all levels. © *1998 American Institute of Physics.*
[S0021-8979(98)10013-0]

I. INTRODUCTION

Glow discharges are used in a range of application fields: in the microelectronics industry for thin film deposition and plasma etching, as plasma display panels, as metal vapor ion lasers, as fluorescent lamps, and also in analytical chemistry, as spectroscopic sources for mass spectrometry and optical emission spectrometry. In the latter application, the cathode of the glow discharge is constructed from the material to be analyzed; the cathode is bombarded by the plasma particles (predominantly fast argon atoms and argon ions), and the sputtered (analytically important) atoms arrive in the plasma where they can be ionized or excited, making the glow discharge useful as source for mass spectrometry and optical emission spectrometry.[1,2]

In the past, we have been modeling a glow discharge used as an ion source for mass spectrometry (see e.g., Refs. 3–10), i.e., with special emphasis on the ionization of argon and sputtered atoms, and on the behavior of these ions. However, we would now like to extend our modeling work to the application of glow discharges for optical emission spectrometry, i.e., by calculating the optical emission profiles and the behavior of the various excited levels. This topic can be studied by so-called collisional-radiative (CR) models, i.e., the level populations of the different excited states are determined by a range of collisional and radiative processes. A number of CR models have been reported in the literature, e.g., Refs. 11–23. An excellent review of CR models in different types of plasmas is presented in Ref. 18. CR models are not only utilized for studying the population distribution over the different excited states; they give also information about the relative importance of the different populating and depopulating processes. Moreover, they are also useful for plasma diagnostic studies (determination of temperatures from the intensities of spectral lines), and they are of fundamental importance for modeling light sources.

In most CR models, a Maxwellian energy distribution is assumed for the electrons.[11–20] However, this assumption is not justified in the analytical glow discharges which we like to describe and which operate at voltages of about 1 kV; indeed, the electrons have an energy distribution ranging from thermal to maximum energy (e.g., 1000 eV).[3,4] Therefore, we use a Monte Carlo (MC) model for the electrons to calculate the electron energy distribution, and this MC model is combined with a CR model for argon. The electron MC model was developed before,[3,4] but has been extended here to a wide range of other collision processes which are relevant for the CR model (i.e., detailed excitation and deexcitation between different levels, and ionization and recombination for all these levels; see below).

The CR model presented in this article is an extension of the model of Vlcek,[21] with a more detailed analysis of the two 4*s* metastable levels, and with the incorporation of fast argon ion and atom impact ionization and excitation between the different levels. Indeed, it was shown that in glow discharges which operate at voltages of about 1 kV, fast argon ion and atom impact ionization and excitation play an important role close to the cathode, in the region called ''cathode dark space'' (CDS), where a strong electric field is present and where the argon ions and argon atoms (created from the argon ions by symmetric charge transfer and elastic collisions) can reach high energies.[5,6,10,24–26] Therefore, a MC model for argon ions and fast argon atoms has been developed here, incorporating detailed fast argon ion and atom impact excitation and deexcitation, and ionization and recombination for all the levels, and the results are used as input in the present CR model.

The setup of our CR model is described in Sec. II, and a discussion about the basic data is given in Sec. III. Section

[a]Author to whom correspondence should be addressed; electronic mail: bogaerts@uia.ua.ac.be

IV presents the typical results, i.e., the level populations of the various excited states and the relative importance of the different populating and depopulating processes.

II. DESCRIPTION OF THE MODEL

The present CR model forms part of a comprehensive modeling network with different submodels for the various species present in the glow discharge. The plasma is assumed to consist of thermal argon atoms in the ground state and in different excited levels, argon ions in the ground state [more or less thermalized in the negative glow (NG), and with somewhat higher kinetic energies in the CDS], fast argon atoms in the ground state in the CDS, electrons with energies ranging from thermal to maximum energy (i.e., 1000 eV for a 1 kV discharge voltage), and sputtered atoms. The latter play a role in a loss process for the argon metastable atoms, by Penning ionization (see below and Refs. 6 and 10).

All these species are described by a combination of MC and fluid models. The behavior of the electrons throughout the discharge, and of the argon ions and fast argon atoms in the CDS is described with a MC model[3–5,7] (see also Sec. III). Further, the argon ions are also treated with a fluid model throughout the discharge, together with a group of thermalized electrons;[4,7] the balance and transport equations of this model are coupled to the Poisson equation, and a self-consistent electric field is calculated, which is used to describe the behavior of the electrons, argon ions and fast argon atoms with the MC model. The behavior of the sputtered atoms, i.e., thermalization after sputtering from the cathode, further diffusion, ionization (by Penning ionization due to argon metastable atoms, asymmetric charge transfer due to argon ions, and electron impact ionization), and the transport of the created ions are described with a combination of two MC simulations and one fluid model, as is explained in detail in Refs. 8–10. Finally, the various excited levels of the argon atom are handled with a CR model, as will be described in detail in the present article.

Figure 1 shows an energy level diagram of argon, with the 65 discrete effective levels used in the model.[21] Only excited levels due to one electron excitation are incorporated in the model. The ground state and the four $4s$ levels are considered separately, the higher levels are grouped into effective levels according to their excitation energy and their core quantum number (j_c). Indeed, the levels are divided into two subsystems, with two different ionization limits: the ''primed'' system ($j_c=1/2$, corresponding to the ionization limit $^2P_{1/2}$ in Ar^+) and the ''unprimed'' system ($j_c=3/2$, with ionization limit $^2P_{3/2}$ in Ar^+). The effective levels are indicated with the effective level number n. The designation (according to Moore),[27] the excitation energy and the statistical weights of these effective levels are also listed in Table I. The collisional and radiative processes taken into account in the model are the following:

(1) Electron impact excitation and de-excitation between all the levels.
(2) Fast argon ion impact excitation and de-excitation between all the levels, in the CDS.

TABLE I. Effective level numbers (n) of the 65 levels incorporated in the model, together with their designation (according to Moorè Ref. 27), their effective excitation energy and the total statistical weight.

Effective level number: n	Designation	Excitation energy (eV)	Statistical weight
1	$3p^6\,{}^1S$	0.0	1
2	$4s[3/2]_2$	11.548	5
3	$4s[3/2]_1$	11.624	3
4	$4s'[1/2]_0$	11.723	1
5	$4s'[1/2]_1$	11.828	3
6	$4p[1/2]_1$	12.907	3
7	$4p[3/2]_{1.2}+[5/2]_{2.3}$	13.116	20
8	$4p'[3/2]_{1.2}$	13.295	8
9	$4p'[1/2]_1$	13.328	3
10	$4p[1/2]_0$	13.273	1
11	$4p'[1/2]_0$	13.480	1
12	$3d[1/2]_{0.1}+[3/2]_2$	13.884	9
13	$3d[7/2]_{3.4}$	13.994	16
14	$3d'[3/2]_2+[5/2]_{2.3}$	14.229	17
15	$5s'$	14.252	4
16	$3d[3/2]_1+[5/2]_{2.3}+5s$	14.090	23
17	$3d'[3/2]_1$	14.304	3
18	$5p$	14.509	24
19	$5p'$	14.690	12
20	$4d+6s$	14.792	48
21	$4d'+6s'$	14.976	24
22	$4f'$	15.083	28
23	$4f$	14.906	56
24	$6p'$	15.205	12
25	$6p$	15.028	24
26	$5d'+7s'$	15.324	24
27	$5d+7s$	15.153	48
28	$5f',g'$	15.393	64
29	$5f,g$	15.215	128
30	$7p'$	15.461	12
31	$7p$	15.282	24
32	$6d'+8s'$	15.520	24
33	$6d+8s$	15.347	48
34	$6f',g',h'$	15.560	108
35	$6f,g,h$	15.382	216
36	$8p'$	15.600	12
37	$8p$	15.423	24
38	$7d'+9s'$	15.636	24
39	$7d+9s$	15.460	48
40	$7f',g',h',i'$	15.659	160
41	$7f,g,h,i$	15.482	320
42	$8d',f',\ldots$	15.725	240
43	$8d,f,\ldots$	15.548	480
44	$9p',d',f',\ldots$	15.769	320
45	$9p,d,f,\ldots$	15.592	640
46	$10s',p',d',f',\ldots$	15.801	400
47	$10s,p,d,f,\ldots$	15.624	800
48	$11s',p',d',f',\ldots$	15.825	484
49	$11s,p,d,f,\ldots$	15.648	968
50	$12s',p',d',f',\ldots$	15.843	576
51	$12s,p,d,f,\ldots$	15.666	1152
52	$13s',p',d',f',\ldots$	15.857	676
53	$13s,p,d,f,\ldots$	15.680	1352
54	$14s',p',d',f',\ldots$	15.868	784
55	$14s,p,d,f,\ldots$	15.691	1568
56	$15s',p',d',f',\ldots$	15.877	900
57	$15s,p,d,f,\ldots$	15.700	1800
58	$16s',p',d',f',\ldots$	15.884	1024
59	$16s,p,d,f,\ldots$	15.707	2048
60	$17s',p',d',f',\ldots$	15.890	1156
61	$17s,p,d,f,\ldots$	15.713	2312
62	$18s',p',d',f',\ldots$	15.895	1296
63	$18s,p,d,f,\ldots$	15.718	2592
64	$19s',p',d',f',\ldots$	15.899	1444
65	$19s,p,d,f,\ldots$	15.722	2888

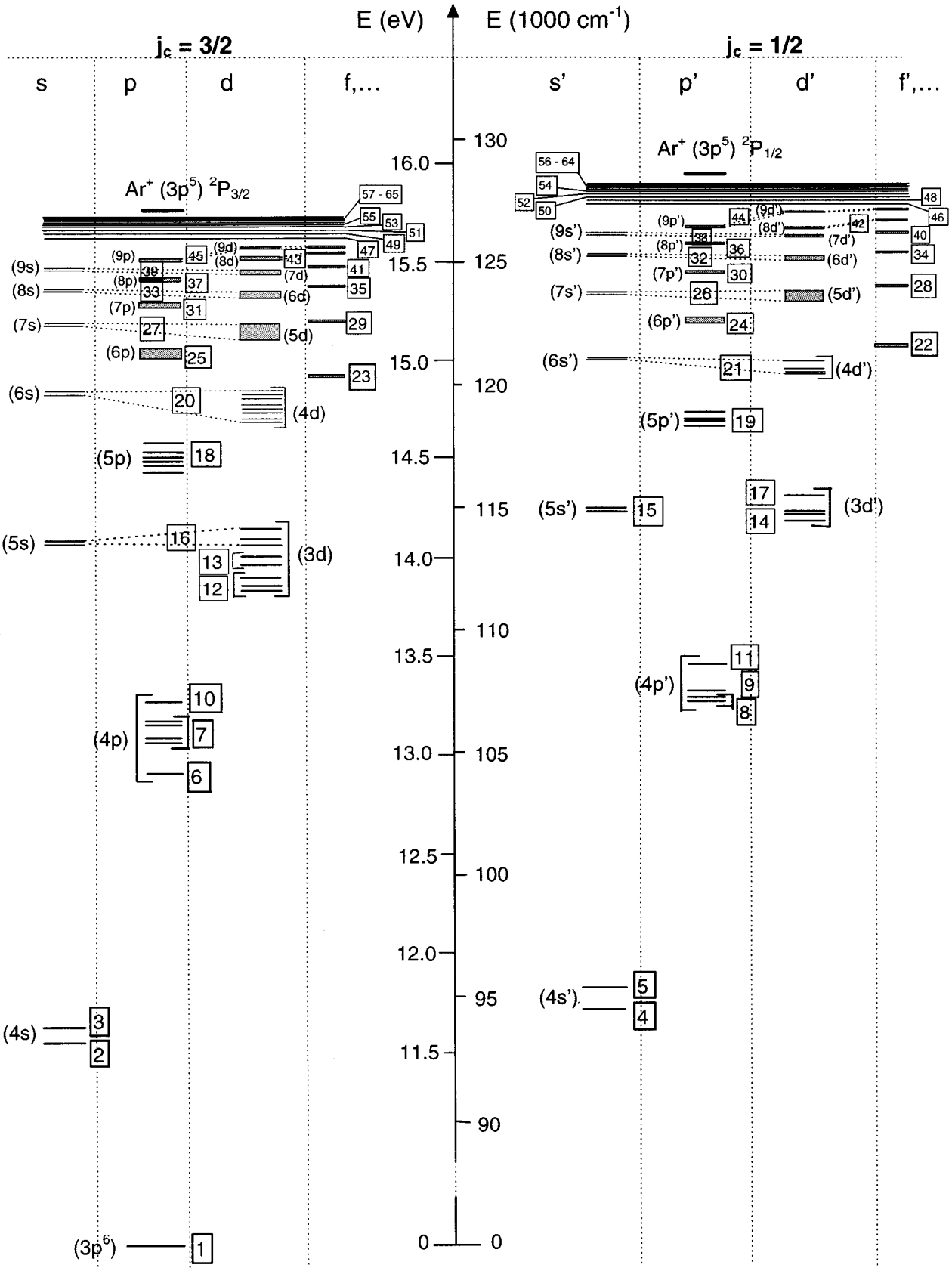

FIG. 1. Energy level scheme of the argon atom, illustrating all the effective levels incorporated in the model.

(3) Fast argon atom impact excitation and de-excitation between all the levels, in the CDS.

(4) Thermal argon atom impact excitation and de-excitation between all the levels. (Excitation and de-excitation by thermal argon ions in the NG is neglected, since the density of these ions is 4 to 5 orders of magnitude lower than the thermal argon atom density.[4,7])

(5) Radiative decay (and photo-excitation) between all the levels.
(6) Electron impact ionization from, and three-body recombination to all levels [the third body is an electron].
(7) Fast argon ion impact ionization from all levels, and three-body recombination to all the levels [the third body is a fast argon ion], in the CDS.
(8) Fast argon atom impact ionization from all levels, and three-body recombination to all levels [the third body is a fast argon atom], in the CDS.
(9) Thermal argon atom impact ionization from all levels, and three-body recombination to all levels [the third body is a thermalized argon atom in the ground state]. (The corresponding processes by thermal argon ions in the NG are not considered, due to their much lower density.)
(10) Radiative recombination to (and photoionization from) all the levels.

The net rate of radiative decay (process 5) is given by the Einstein transition probability, multiplied by an ''escape factor'' (Λ), describing the effect of ''radiation trapping''.[28–31] Indeed, a fraction of the emitted radiation from an upper (m) to a lower (n) level can again be absorbed by the lower level, leading to re-excitation from the lower to the upper level, i.e., called ''radiative excitation or photoexcitation.'' This effect is only important when the lower level is the atom ground state, since the number density of the ground state is many orders of magnitude higher than the excited level number densities (Ref. 32 and see further). As will be shown later, when the lower level n is 1, $\Lambda(m,1)$ is of the order of 10^{-3}, whereas $\Lambda(m,n)(n\neq 1)$ can be taken equal to 1. Hence, photoexcitation can be neglected for the excited levels ($n>1$). For radiative recombination and photoionization, a similar reasoning can be applied. To avoid the complex problem of radiation transfer, photoionization is also accounted for by means of the escape factors $\Lambda(n)$. For $n=1$, $\Lambda(1)$ is taken as the minimum of all $\Lambda(m,1)$ values, and the rate of photoionization is given by: $R_{\text{ion}ph}=[1-\Lambda(1)]*R_{\text{rad.recomb}}$. For $n>1$, $\Lambda(n)$ can again be assumed to be equal to 1 (due to the much lower population densities), and photoionization can be neglected.

Some additional processes are incorporated for the two $4s$ metastable levels (level $n=2$ and 4):

(11) Penning ionization of sputtered atoms (copper is taken as an example): $\text{Ar}(n)+\text{Cu}^0 \overset{Rpi}{\rightarrow} \text{Ar}^0+\text{Cu}^+ + e^-$.
(12) Two-body collisions with thermal argon ground state atoms. This leads, in principle, to (i) collision induced emission and (ii) collision transfer to the nearby resonant levels. However, it is claimed in the literature[33–35] that collision induced emission is the dominant process. Since collision transfer to the resonant levels is already described by process 4, only collision induced emission is considered here:

$$\text{Ar}(n)+\text{Ar}^0 \overset{R2b}{\rightarrow} \text{Ar}^0+\text{Ar}^0+h\nu.$$

(13) Three-body collisions with thermal argon ground state atoms, leading to the formation of Ar_2^*.
(14) Metastable atom-metastable atom collisions, leading to the ionization of one of the atoms.
(15) Diffusion and subsequent deexcitation at the walls. For the other (nonmetastable) excited levels diffusion may be neglected with respect to the collisional and radiative processes (see the use of the quasistationary state model discussed in greater detail in Refs. 11 and 36).

The level populations of the different excited levels ($n=2-65$) are calculated with a set of coupled balance equations describing all the different collisional and radiative processes. The balance equations are one dimensional, since it was shown[37] that for the typical glow discharge cells used in analytical chemistry (cell radius and cell length of comparable dimensions), the results of one-dimensional models are in good agreement with three-dimensional modeling results. The population of the ground state ($n=1$) is simply calculated by the ideal gas law from the pressure and gas temperature, since the different collisional and radiative processes have a negligible effect on the overall argon atom density.

The balance equations for the excited levels are given by:

$$\frac{dN(n)}{dt}+\frac{dJ(n)}{dz}=R_{\text{prod}}(n,z)-R_{\text{loss}}(n,z),$$

where N is the population density of the levels, J is their flux, and R_{prod} and R_{loss} comprise all production (populating) and loss (depopulating) processes, respectively. The production occurs by electron, fast argon ion, fast argon atom, and thermal argon atom impact excitation from all lower levels (1), by electron, fast argon ion, fast argon atom, and thermal argon atom impact de-excitation and radiative decay from all higher levels (m), by radiative electron-ion recombination and by three-body electron-ion recombination where the third body is an electron, fast argon ion, fast argon atom or thermal argon atom:

$$R_{\text{prod}}(n,z)=\sum_{l=1}^{n-1}\left[R_{\text{exc},e}(l,n,z)+R_{\text{exc},i}(l,n,z)+R_{\text{exc},a}(l,n,z)+R_{\text{exc},th}(l,n,z)\right]$$
$$+\sum_{m=n+1}^{65}\left[R_{\text{de-exc},e}(m,n,z)+R_{\text{de-exc},i}(m,n,z)+R_{\text{de-exc},a}(m,n,z)+R_{\text{de-exc},th}(m,n,z)+\Lambda(m,n)*A(m,n)\right]$$
$$+\Lambda(n)*R_{\text{rad.recomb}}(n,z)+R_{3b\text{recomb},e}(n,z)+R_{3b\text{recomb},i}(n,z)+R_{3b\text{recomb},a}(n,z)+R_{3b\text{recomb},th}(n,z).$$

The loss includes electron, fast argon ion, fast argon atom, and thermal argon atom impact excitation to all higher levels (m),

electron, fast argon ion, fast argon atom and thermal argon atom impact de-excitation, and radiative decay to all lower levels (1), and electron, fast argon ion, fast argon atom, and thermal argon atom impact ionization. For the metastable levels, radiative decay is of course not included. However, these levels can also be depopulated by Penning ionization of sputtered atoms, two- and three-body collisions with argon ground state atoms and metastable atom-metastable atom collisions.

$$R_{\text{loss}}(n,z)=\sum_{m=n+1}^{65}\left[R_{\text{exc},e}(n,m,z)+R_{\text{exc},i}(n,m,z)+R_{\text{exc},a}(n,m,z)+R_{\text{exc},th}(n,m,z)\right]$$
$$+\sum_{l=1}^{n-1}\left[R_{\text{de-exc},e}(n,l,z)+R_{\text{de-exc},i}(n,l,z)+R_{\text{de-exc},a}(n,l,z)+R_{\text{de-exc},th}(n,l,z)+\Lambda(n,l)*A(n,l)\right]$$
$$+R_{\text{ioniz},e}(n,z)+R_{\text{ioniz},i}(n,z)+R_{\text{ioniz},a}(n,z)+R_{\text{ioniz},th}(n,z)+R_{pi}(n,z)+R_{2b}(n,z)+R_{3b}(n,z)+R_{\text{met}}(n,z).$$

The symbols used for all the processes are the following: $R_{\text{exc},e}/R_{\text{exc},i}/R_{\text{exc},a}/R_{\text{exc},th}$, $R_{\text{de-exc},e}/R_{\text{de-exc},i}/R_{\text{de-exc},a}/R_{\text{de-exc},th}$, and $R_{\text{ioniz},e}/R_{\text{ioniz},i}/R_{\text{ioniz},a}/R_{\text{ioniz},th}$ are the rates of electron, fast argon ion, fast argon atom and thermal argon atom impact excitation, de-excitation and ionization; $R_{\text{rad,recomb}}/R_{3b\text{recomb},e}/R_{3b\text{recomb},i}/R_{3b\text{recomb},a}/R_{3b\text{recomb},th}$ are the rate of radiative recombination and three-body recombination where the third body is an electron, fast argon ion, fast and thermal argon atom; A and Λ are the Einstein transition probability and escape factor, resp.; and $R_{pi}/R_{2b}/R_{3b}/R_{\text{met}}$ are the rates for Penning ionization, two- and three-body collisions with argon ground state atoms, and metastable atom-metastable atom collisions.

An additional loss process is given by the transport term (diffusion and subsequent de-excitation at the walls):

$$\frac{dJ(n)}{dz}=-D\,\frac{d^2N(n)}{dz^2}.$$

This term is only important for the metastable levels ($n=2,4$). For the other levels, it can be neglected with respect to the collisional and radiative processes, as mentioned before.

Since the population of level n is determined by the higher and lower levels due to excitation and de-excitation, the 64 balance equations for the 64 effective excited levels ($n=2-65$) are solved simultaneously at each time step, until convergence is reached.

III. DISCUSSION OF THE BASIC DATA

A. Electron induced processes

As mentioned before, at the typical glow discharge conditions studied here, the electrons are not characterized by a Maxwellian energy distribution but they have energies ranging from thermal to maximum energy (e.g., 1000 eV for a 1 kV discharge voltage). Therefore, we describe their behavior with a MC model taking into account all collision processes mentioned above (i.e., electron impact excitation and de-excitation between all 65 levels, electron impact ionization from all levels, electron-ion radiative recombination and electron-ion three-body recombination where the third body is an electron). Moreover, elastic collisions with argon atoms and electron-electron Coulomb scattering are also incorporated. The latter process affects largely the electron energy distribution at low energies.[38,39] Collisions with the sputtered copper atoms are not included here. They were, however, taken into account in our previous versions of the MC model, but it was found that for the discharge conditions under study the copper atoms are of minor importance (its density is 4 orders of magnitude lower than the argon atom density),[9,10] and hence they have a negligible effect on the electron energy distribution. Similarly, electron–argon ion interactions were neglected in this MC model, because the argon ion density is about 4 to 5 orders of magnitude lower than the argon atom density[4,7] and collisions with argon ions can, therefore, be considered of minor importance.

The electron MC model follows all electrons which started at the cathode by secondary electron emission, and the electrons formed in the glow discharge plasma by electron, fast argon ion and atom impact ionization. The principles of the present electron MC model are the same as for our previous MC model, and the details can be found in Refs. 3, 4, and 7. The only differences with our previous model are the following: (i) the electrons are not transferred to the thermal electron group (described in a fluid model)[4,7] when their energy is lower than a certain threshold energy but the entire electron population is described by the MC model, and (ii) new collision processes are added to the model (i.e., detailed excitation, de-excitation, ionization, and recombination for all 65 levels, as well as electron–electron Coulomb scattering.

The cross sections for electron impact ionization from the different effective levels n, as a function of the electron energy were calculated from:[21]

$$\sigma(n,E)=4\pi a_0^2\left(\frac{\epsilon_1^H}{E_{\text{ioniz}}(n)}\right)^2\xi_n\alpha_n\left(\frac{E}{E_{\text{ioniz}}(n)}\right)^{-2}\times\left(\frac{E}{E_{\text{ioniz}}(n)}-1\right)\ln\left(1.25\beta_n\,\frac{E}{E_{\text{ioniz}}(n)}\right),$$

where a_0 is the first Bohr radius of the hydrogen atom, ϵ_1^H is the ionization energy for atomic hydrogen in the ground state, $E_{\text{ioniz}}(n)$ is the ionization energy of the effective level n, ξ_n is the number of energetically equivalent electrons in shell n ($\xi_n=6$ for $n=1$ and $\xi_n=1$ for $n>1$), and α_n and β_n are level-dependent parameters.[21] The cross section for electron impact ionization from the ground state ($n=1$) is, however, adopted from Refs. 40 and 41, because of the availabil-

ity of a differential ionization cross section (calculation of the energies of the primary and secondary electrons):

$$\sigma(n=1,E)=10^{-16}\frac{23.9}{E}\ln\left(\frac{E+\frac{150}{E}}{E_{\text{ioniz}}(n=1)}\right)\times 4.6\left\{\arctan\left(\frac{a-\epsilon}{4.6}\right)-\arctan\left(\frac{-\epsilon}{4.6}\right)\right\},$$

where $a=[E-E_{\text{ioniz}}(n=1)]/2$, and $\epsilon=1.2-250/[E+2E_{\text{ioniz}}(n=1)]$. For electron impact ionization from the excited levels we did not use a differential cross section but the energy is simply divided between the primary and secondary electron based on a random number (RN):

$$E_{\text{prim}}=\text{RN}(E-E_{\text{ioniz}}(n)),$$

and

$$E_{\text{sec}}=(1-\text{RN})(E-E_{\text{ioniz}}(n)).$$

This assumption is justified since ionization from the excited levels is many orders of magnitude lower than ionization from the ground state and it does not affect the electron energy.

These empirical cross sections were compared with experimental values when available. The ionization cross section from the ground state ($n=1$) is in excellent agreement with the experimental results of Rapp *et al.*,[42] and the cross sections for ionization from the $4s$ and $4p$ states ($n=2-11$) are in satisfactory agreement with the experimental data presented by Hyman,[43] as was also shown in Ref. 21. For the more excited levels, we are not aware of experimental data.

The cross sections for electron impact excitation between the levels are also taken from Ref. 21:

$$\sigma(n,m,E)=\sigma^A(n,m,E)+\sigma^F(n,m,E),$$

where n and m denote the lower and upper level, respectively, E is the electron energy, and σ^A and σ^F symbolize the cross sections for optically allowed ($\Delta l=\pm 1$, $\Delta J=0,\pm 1$, but not $J=0\rightarrow J=0$), and forbidden transitions, respectively:

$$\sigma^A(n,m,E)=4\pi a_0^2\left(\frac{\epsilon_1^H}{E_{mn}}\right)^2 f_{mn}\alpha_{mn}^A\left(\frac{E}{E_{mn}}\right)^{-2}\times\left(\frac{E}{E_{mn}}-1\right)ln\left(1.25\beta_{mn}\frac{E}{E_{mn}}\right),$$

$$\sigma^F(n,m,E)=\sigma^P(n,m,E)=4\pi a_0^2\alpha_{mn}^P\left(\frac{E}{E_{mn}}\right)^{-1}\left(1-\left(\frac{E}{E_{mn}}\right)^{-1}\right),$$

or

$$\sigma^F(n,m,E)=\sigma^S(n,m,E)=4\pi a_0^2\alpha_{mn}^S\left(\frac{E}{E_{mn}}\right)^{-3}\left(1-\left(\frac{E}{E_{mn}}\right)^{-2}\right),$$

where E_{mn} is the energy difference between level m and level n ($E_{mn}=E_m-E_n$), f_{mn} is the oscillator strength of the transition, α_{mn} and β_{mn} are transition-dependent parameters, and P and S reflect the parity- and spin-forbidden transitions, respectively. For the optically allowed transitions ($\Delta l=\pm 1$, $\Delta J=0,\pm 1$, but not $J=0\rightarrow J=0$), intercombination transitions between the primed ($^2P_{1/2}$) and unprimed ($^2P_{3/2}$) system are taken into account for $2\leqslant n<m\leqslant 45$, but they are neglected for $2\leqslant n\leqslant 45<m\leqslant 65$ and $45\leqslant n<m\leqslant 65$. Moreover, the parity forbidden transitions ($\Delta l\neq\pm 1$) are only considered within the primed or unprimed system (no intercombination transitions) for $2\leqslant n<m\leqslant 45$ (except for the transitions between the first four excited states, where intercombination transitions are included; see below), and they are totally neglected for higher transitions. Indeed, when $\Delta l\neq\pm 1$, the rules $\Delta J>1$ or $J=0\rightarrow J=0$, or the intercombination between primed and unprimed system represent further bans for a transition, and the cross sections are therefore expected to be very small. The semiempirical formula are originally proposed by Drawin;[44] they have also been extensively evaluated by Kimura *et al.*,[45] and they have been discussed by Vlcek as well,[21] so that we refer to these papers for more information.

The above formula were used for all possible transitions, except for the optically forbidden transitions between the first four excited levels, where we used the following cross sections:[21]

$$\sigma(n,m,E)=\frac{g_m}{g_n}\frac{E-E_{mn}}{E}5.797\times 10^{-15}\times Q_{nm}(E-E_{mn})^{-0.54},$$

where

$$Q_{23}=1,\quad Q_{24}=Q_{25}=Q_{34}=Q_{35}=0.1,$$

and for $n=4$, $m=5$;

$$\sigma(n,m,E)=\frac{g_m}{g_n}\frac{E-E_{mn}}{E}8.111\times 10^{-16}(E-E_{mn})^{-1.04}.$$

The cross sections for electron impact de-excitaton between the effective levels are obtained from the corresponding cross sections for electron impact excitation, based on the principle of detailed balancing:

$$e^-(E)+\text{Ar}(n)\underset{\text{de-excit}}{\overset{\text{excit}}{\rightleftarrows}}e^-(E')+\text{Ar}(m),$$

$$\sigma_{\text{de-excit}}(m,n,E')=\frac{g_nE}{g_mE'}\sigma_{\text{excit}}(n,m,E),$$

where $E'=E-E_{mn}$, and g_n and g_m are the level degeneracies of the lower and upper level, respectively.

The cross sections for three-body electron-argon ion recombination to the 65 effective levels (when the third body is an electron) are obtained from the electron impact ionization cross sections, in a manner similar as for electron excitation/de-excitation:

$$e^-(E)+\text{Ar}(n)\underset{3b\text{-recomb}}{\overset{\text{ioniz}}{\rightleftarrows}}e^-(E')+\text{Ar}^+ +e_b^-(E_b),$$

where $E'=E-E_{\text{ioniz}}(E)-E_b$, and e_b^- is the originally bound electron. A precise description of three-body recombination leads to the conversion formula between the differ-

ential cross sections for ionization and three-body recombination, $\sigma_{\text{ioniz}}(n,E,E_b)$ and $\sigma_{3b-\text{recomb}}(n,E',E_b)$, which depend on the energy of the bound electron, E_b. However, when assuming $E_b=0$, the conversion formula between $\sigma_{\text{ioniz}}(n,E)$ and $\sigma_{3b\text{-recomb}}(n,E')$ can be written as:

$$\sigma_{3b-\text{recomb}}(n,E')\,\frac{1}{n_e} = \frac{g_n}{2g_1^+}\left(\frac{h^2}{2\pi m_e kT_e}\right)^{3/2}\frac{E}{E'}\,\sigma_{\text{ioniz}}(n,E),$$

where $E'=E-E_{\text{ioniz}}(n)$, n_e is the electron density, g_1^+ is the statistical weight of the ion ground state (i.e., different for the primed and unprimed system: $g_1^+=6$ when $n=1$ (atom ground state), $g_1^+=4$ or 2 when the atom level n belongs to the unprimed ($^2P_{3/2}$) or primed ($^2P_{1/2}$) system, respectively), h is the Planck constant, m_e is the electron mass, k is the Boltzmann constant, and T_e corresponds to the mean electron energy in the glow discharge.

The cross section for electron-argon ion radiative recombination is again deduced from its inverse process, i.e., photoionization:

$$\text{Ar}(n)+h\nu \underset{\text{rad.recomb}}{\overset{\text{photoioniz}}{\rightleftarrows}} \text{Ar}^+ + e^-(E),$$

$$\sigma_{\text{rad.recomb}}(n,E)=\frac{g_n}{2g_1^+}\frac{(h\nu)^2}{m_e c^2}\frac{1}{E}\,\sigma_{\text{photoioniz}}(n,h\nu),$$

where $E=h\nu-E_{\text{ioniz}}(n)$, c is the speed of light, $h\nu$ is the photon energy responsible for photoionization, and the cross section for photoionization was presented in Ref. 21.

Finally, the cross section for electron elastic collisions with argon atoms is taken from Refs. 46 and 47, and the one for electron–electron Coulomb scattering is adopted from Ref. 39. The cross section of electron–electron Coulomb scattering is very high, especially at low energies (i.e., 10^{-7} cm^2 at 0.01 eV dropping to about 3×10^{-17} cm^2 at 1000 eV), and since the energy transfer between two electrons is very efficient due to their equal mass, it can be expected that this process has a large effect on the electron energy at low energies. Nevertheless, it must be taken into account that the density of the target particle (i.e., electrons) is many orders of magnitude lower than the argon ground state atom density (i.e., $n_e\sim10^{11}-10^{12}$ cm^{-3} and $n_{\text{Ar}}\sim10^{16}$ cm^{-3}), so that this process is, in practice, only important at electron energies of a few eV and lower.

The electron energy distribution calculated with this detailed MC model is indeed characterized by energies ranging from 0 to 1000 eV, but in the NG most electrons have rather low energies (around 0.4 eV), as is shown, e.g., in Ref. 48.

B. Fast argon ion and atom induced processes

Since it was demonstrated before[5,6,10,24–26] that fast argon ions and atoms can produce a rather large amount of ionization and excitation in the CDS close to the cathode, the ionization and excitation processes induced by these species are also included in our model. The behavior of the fast argon ions and atoms in the CDS (this is the only region where they are actually present) is also calculated with a MC model. The collision processes described in the MC model include fast argon ion and atom impact excitation and deexcitation between all 65 levels, ionization from the levels, and electron-ion three-body recombination where the third body is a fast argon ion or atom. Additional collision processes incorporated, are elastic collisions with thermal argon atoms, for both argon ions and atoms, and symmetric charge transfer collisions for the argon ions. Since the latter process is a collision between an atom and ion of the same kind (i.e., argon), the argon ion is formed in the ground state, which gives perfect energy resonance. This is in contrast to asymmetric charge transfer between argon ions and (e.g.) copper atoms, in which copper ions are mainly formed in excited levels, because this yields a higher cross section due to energy resonance.

It should be mentioned that the term ''fast'' is used for all argon ions in the CDS; indeed, when they are slowed down after a collision, they gain almost immediately energy again from the electric field. On the other hand, ''fast argon atoms'' are those with energies higher than thermal energy; when they reach a certain threshold of 0.06 eV (i.e., the thermal atom energy at the assumed gas temperature of 450 K), they are transferred to the thermal argon atom group.

The principles of this MC model are the same as for the previously developed argon ion and fast argon atom MC model[3,5,7] but again complemented with detailed excitation, de-excitation, ionization, and recombination for all 65 levels.

The cross sections for elastic collisions of the argon ions and atoms as a function of the argon ion and atom energies are taken from Ref. 49, like in our previous model.[7] It should be mentioned that the elastic collisions for the ions include also symmetric charge transfer. Indeed, there is no change in kinetic energy of the collision partners, only an electron is transferred; therefore this process is also called ''elastic''.[49] The cross sections for argon ion and atom impact ionization from the 65 effective levels were proposed by Drawin and Emard:[21,50]

$$\sigma_{\text{ioniz}}(n,E)=4\pi a_0^2\left(\frac{\epsilon_1^H}{E_{\text{ioniz}}(n)}\right)^2\frac{m_{\text{Ar}}}{m_{\text{H}}} \times\xi_n^2\frac{2m_e}{m_e+m_{\text{Ar}}}\left(\frac{E}{E_{\text{ioniz}}(n)}-1\right) \times\left[1+\frac{2m_e}{m_e+m_{\text{Ar}}}\left(\frac{E}{E_{\text{ioniz}}(n)}-1\right)\right]^{-2},$$

where m_{H}, m_{Ar}, and m_e are the masses of hydrogen and argon atoms and of electrons, respectively, and the other symbols have been explained before. For ionization from the ground state level, however, we used the experimental cross sections, recommended by Phelps.[51] At high energies, these cross sections are of comparable magnitude to the corresponding cross sections for electron impact ionization.

The cross sections for argon ion and atom impact excitation between the 65 levels are taken similar to the cross sections for argon ion and atom impact ionization (see above), but the ionization energy $[E_{\text{ioniz}}(n)]$ is replaced by the energy difference between the levels $[E_{mn}=E_{\text{excit}}(m)-E_{\text{excit}}(n)]$, and the cross section is multiplied by the oscillator strength, f_{mn}.[21,50] It should be mentioned that this for-

mula yields only nonzero values for the cross sections when $f_{mn} \neq 0$, i.e., for optically allowed transitions. For argon ion and atom impact excitation from the ground state, this formula computes, therefore, a cross section equal to zero for excitation to the $4p$ states, whereas it is demonstrated experimentally that the cross sections for these excitation transitions can be rather high.[25,26,51,52] Therefore, for excitation from the ground state, we have used the data of Phelps:[51] for excitation to the four $4s$ levels ($n=2-5$) we used the cross sections for UV excitation, whereas excitation to the $4p$ levels is represented by the cross sections of 811 and 795 nm emission. For excitation to higher levels, it was found in Ref. 52 that the total cross section for $5p$ excitation and for $4d$ excitation is a fraction of 0.03 and 0.1 of the total cross section for $4p$ excitation, resp. The total cross section for excitation to the $5d$ levels is $0.02^{*}\sigma_{4p}$, and σ_{6d} and σ_{7d} are $0.01^{*}\sigma_{4p}$. The cross sections for excitation to the higher lying ns ($n \geqslant 5$) and np ($n \geqslant 6$) levels were estimated to be about one order of magnitude smaller than those for the corresponding nd levels. We have not found any data for excitation to the $3d$ levels, but based on their excitation energy we take the cross sections intermediate to the cross sections for $4p$ and $5p$ excitation. Only excitation to the effective levels $n \leqslant 21$ are taken into account; excitation to higher levels may be assumed to be negligible in the energy range of interest to us. Although the results of the empirical formula of the excitation cross sections[21,50] are not in complete agreement with these experimental cross sections (e.g., the cross sections to the $4p$ levels are calculated to be zero with the empirical formula), the absolute values of the other calculated cross sections are in reasonable agreement with the experimental values, which is a validation of the empirical formula. This empirical formula is therefore used for excitation between the excited levels (also due to the lack of other experimental data).

The cross sections for argon ion and atom impact deexcitation are deduced from the corresponding cross sections for excitation, based on the principle of detailed balancing, similar as for the electrons (see above). At high energies the cross sections for argon ion and atom impact excitation and de-excitation become again comparable to the corresponding cross sections for electron impact excitation and deexcitation.

The cross sections for electron-argon ion three-body recombination, where the third body is an argon ion or fast argon atom, are again obtained from the cross sections for argon ion and atom impact ionization, in analogy to the electron cross sections.

From running this MC model, it follows that the calculated energy distributions of fast argon ions and atoms decrease clearly towards higher energy (see e.g., Refs. 3 and 48).

C. Thermal argon atom induced processes

The thermalized argon atoms can also give rise to ionization and recombination (three-body electron-ion recombination where the third body is a thermal argon atom) and to excitation and de-excitation between the different levels. Recombination and de-excitation are possible for all levels; ionization and de-excitation can only occur when the energy required for ionization or excitation is lower than the thermal argon atom energy (i.e., about 0.06 eV at the assumed gas temperature of 450 K), and will therefore only play a role for the highly excited levels. The cross sections used for ionization, deexcitation and three-body recombination are the same as for the fast argon atom induced processes (see above). For thermal argon atoms with energies of 0.06 eV, the ionization cross section was calculated to be zero for the levels $n \leqslant 57$; for levels $n<57$ the computed values range from 5×10^{-17} to 3×10^{-16} cm^2.

For excitation, however, we did not use the same formula as for fast argon atom impact excitation, because this formula applies only to allowed transitions and we want to describe here both allowed and forbidden transitions. Therefore, we used the following formula for excitation from level n to level m:

$$\sigma_{\text{excit}}(n,m,E) = b_{nm}[E_{\text{thermal}} - E_{nm}],$$

where E_{nm} is the energy difference between the levels n and m [$E_{nm}=E_{\text{excit}}(m)-E_{\text{excit}}(n)$] and b_{nm} is a level dependent parameter.[21] For all transitions, except those between the lowest four excited levels, $b_{nm}=8.69\times10^{-18}\ (E_{nm})^{-2.26}$; this relation was derived from comparison with experimental cross section data.[21] For the transition between the $4s$ and $4s'$ levels ($n=2-5$) we used:[21] for excitation from $n=2$ to $m=3$ and from $n=4$ to $m=5$: $b_{23}=b_{45}=1.79 \times 10^{-20}(E_{nm})^{-2.26}$; and for excitation from $n=2,3$ to $m=4,5$: $b_{24}=b_{25}=b_{34}=b_{35}=4.8\times10^{-22}(E_{nm})^{-2.26}$; which is based on the results of Tachibana.[53] No further intercombination transitions (between primed and unprimed system) were considered. For thermal argon atoms with energies of 0.06 eV the excitation cross sections were only nonzero for transitions between the highly excited levels and for some lower levels, which are lying close enough to each other (see Fig. 1 and Table I).

D. Radiative decay from higher to lower excited levels

As already mentioned before, the rate of radiative decay is given by the Einstein transition probability, multiplied by an escape factor (Λ), describing the effect of ''radiation trapping.'' The transition probabilities were adopted from Ref. 21 [i.e., calculated on the basis of intermediate and (j,K) coupling]. However, for the $4s-4p$ and $4s-5p$ transitions, which give rise to the two most important groups of Ar I lines in the spectrum, the data recommended by Wiese *et al.*[54] were utilized. The transition probabilities from and towards effective levels were calculated from the individual values by

$$\overline{A}(m,n) = \sum_x \sum_y g(y)A(y,x) \Big/ \sum_y g(y),$$

where n and m are the lower and upper effective levels, and x and y are the individual levels belonging to the lower and upper effective levels, respectively.

The escape factors are assumed to be equal to 1 (i.e., 100% escape of radiation, no radiation trapping) for transitions to the lower levels $n>1$. For transitions to the ground state ($n=1$) the escape factors are calculated as follows:[21,28–30] for a cylindrical tube of radius R, and when both Doppler and collisional line broadening are present, it holds:

$$\Lambda(m,1)=1.9T_D\ \exp\left(\frac{-\pi T_{CD}^2}{4T_C^2}\right)+1.3T_C\ \mathrm{erf}\left(\frac{\sqrt{\pi}T_{CD}}{2T_C}\right),$$

where T_D and T_C are the transmission coefficients for pure Doppler and collisional broadening, respectively, and T_{CD} is the coefficient for collisionally broadened emission and Doppler broadened absorption profiles:

$$T_D=\frac{1}{k_0R\sqrt{\pi\ \ln(k_0R)}};\quad T_C=\sqrt{\frac{a}{\sqrt{\pi}k_0R}};$$

$$T_{CD}=\frac{2a}{\pi\sqrt{\ln(k_0R)}}.$$

k_0R is the optical depth pertaining to the line center and a is the damping coefficient:

$$k_0R=\frac{2.1\times10^{-17}g(m)}{[E_{\mathrm{excit}}(m)]^3\sqrt{T_{\mathrm{gas}}}}A(m,1)N_{\mathrm{gas}}R,$$

$$a=A(m,1)\left[1+\frac{3.225\times10^{-14}}{[E_{\mathrm{excit}}(m)]^3}g(m)N_{\mathrm{gas}}\right]\frac{4.839\times10^{-9}}{E_{\mathrm{excit}}(m)\sqrt{T_{\mathrm{gas}}}}.$$

$E_{\mathrm{excit}}(m)$ and $g(m)$ are the excitation energy and statistical weight of level m, respectively, $A(m,1)$ is the Einstein transition probability for radiative decay from level m to level 1 (the ground state) and T_{gas} and N_{gas} are the argon gas temperature (450 K) and atom density in the ground state, resp. At the pressures usually found in our glow discharges ($\sim$1 Torr) the escape factors were calculated to be typically about 10^{-3}; hence most emitted radiation for transitions to the ground state is reabsorbed and only a small fraction can escape.

E. Additional data corresponding to the two 4*s* metastable levels ($n=2$ and 4)

Finally, some additional processes were included in the model for the two 4*s* metastable levels, similar to our previous model for the argon metastable atoms.[6,10] Rate coefficients for Penning ionization between argon metastable atoms and sputtered metal atoms are very difficult to find in the literature. We used an empirical formula[55] which we fitted to some experimentally obtained cross sections[55,56] in order to arrive at approximate values for other elements. In this way, a rate coefficient of 2.36×10^{-10} cm^3 s^{-1} was obtained for copper, and is assumed the same for both level $n=2$ and $n=4$. The rate coefficients for two- and three-body collisions with thermal argon ground state atoms are adopted from Ref. 53: $k_{2b}=2.3\times10^{-15}$ cm^3 s^{-1} and $k_{3b}=1.4\times10^{-32}$ cm^6 s^{-1} for $n=2$ and $k_{2b}=4.3\times10^{-15}$ cm^3 s^{-1} and $k_{3b}=1.5\times10^{-32}$ cm^6 s^{-1} for $n=4$. The rate coefficient for collisions between two atoms in the metastable levels is taken from Ref. 31: $k_{\mathrm{met}}=6.4\times10^{-10}$ cm^3 s^{-1}. Due to the lack of additional data, it was assumed to be the same for collisions between the two levels $n=2$, the two levels $n=4$ and between level $n=2$ and $n=4$. Finally, the diffusion coefficients for both $n=2$ and $n=4$ are 74.6 cm^2 s^{-1} at 1 Torr and 300 K.[53]

IV. RESULTS AND DISCUSSION

The glow discharge cell to which the model is applied is a cylinder of 2 cm length and 4 cm diameter. The cathode is a disk with diameter of 5 mm at the left end of the cell; the remaining parts of the cell are at anode potential. The MC models were developed in three dimensions and the fluid models in two dimensions, i.e., the three dimensions could be reduced to two dimensions due to the cylindrical symmetry of the cell. The present CR model is, however, only one dimensional, mainly to avoid too large matrices (i.e., populations and relevant processes of 65 levels in three dimensions), and since it was shown before that when cell radius and cell length are of comparable dimensions, the results of one-dimensional models are in good agreement with three-dimensional modeling results.[37] The results will always be presented for typical glow discharge conditions of 1000 V, 1 Torr, and 2 mA.

A. Level populations

Figure 2 illustrates the calculated level populations of the four lowest excited levels of argon, i.e., the $4s[3/2]_2$ metastable level ($n=2$), the $4s[3/2]_1$ nonmetastable level ($n=3$), the $4s'[1/2]_0$ metastable level ($n=4$), and the $4s'[1/2]_1$ nonmetastable level ($n=5$). The $4s[3/2]_2$ metastable level ($n=2$) shows a maximum of about 5×10^{12} cm^{-3} at about 0.06 cm from the cathode and decreases more or less exponentially towards the anode backplate. It reaches zero at the cathode ($z=0$) and at the anode backplate ($z=2$ cm) because the excited levels are assumed to be deexcited at the walls. In a previous work, we have developed a model describing the behavior of the argon metastable ($4s[3/2]_2$) level, in one[6] and in two dimensions,[10] using a balance equation with different production and loss processes. The model was, therefore, similar to the present one, but the behavior of the other excited levels was not calculated explicitly. In Ref. 57 this balance equation model (in two dimensions) was applied to the same cell geometry and discharge conditions as used in the present work. Reasonable agreement is reached between the two models, in spite of their different nature (i.e., accounting explicitly for the other excited levels or not) and a somewhat different set of cross sections used. Indeed, in the previous model, the metastable level density was also characterized by a pronounced peak adjacent to the cathode, although the absolute value was a factor of about 4 lower than the present result. The argon metastable atom density profile was also measured by laser induced fluorescence in the same cell geometry and at the same discharge conditions,[57] and there was also a maximum observed in front of the cathode (although

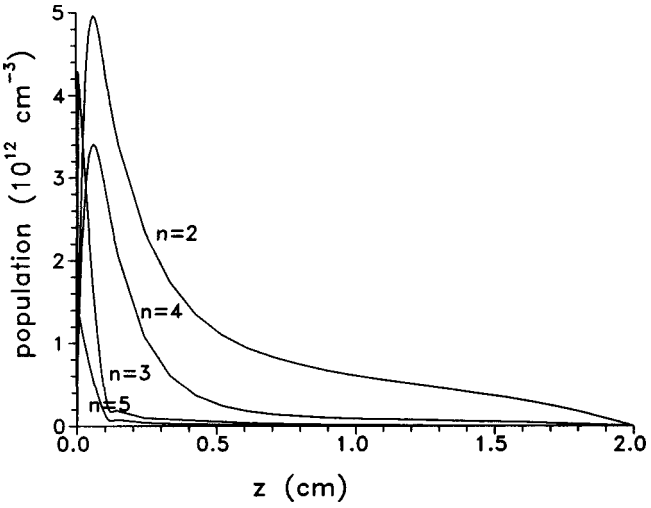

FIG. 2. Calculated level population profiles of the $4s[3/2]_2$ and $4s'[1/2]_0$ metastable levels ($n=2$ and 4, resp.) and the $4s[3/2]_1$ and $4s'[1/2]_1$ nonmetastable levels ($n=3$ and 5, resp.), at 1000 V, 1 Torr, and 2 mA.

this maximum was not so pronounced as in the calculated results). Good agreement is also reached with other experimental profiles for the argon metastable levels presented in Ref. 58. These profiles were recorded for a radio-frequency discharge at different voltages and pressures, and although direct current and radio-frequency discharges can, in principle, not directly be compared, the results at 1 Torr show a peak in front of the cathode and a decrease further in the cell, which are very similar to the present calculation results.

The population profiles of the other $4s,4s'$ excited levels, i.e., the $4s'[1/2]_0$ metastable level ($n=4$) and the $4s[3/2]_1$ and $4s'[1/2]_1$ nonmetastable levels ($n=3$ and 5, resp.), are also depicted in Fig. 2. The $n=4$ metastable level shows qualitatively the same profile as the $4s[3/2]_2$ metastable level. The maximum value is about 3.4×10^{12} cm^{-3}, which is a factor of 1.5 lower than the $n=2$ metastable level. Further away from the cathode, the difference between $n=2$ and $n=4$ becomes larger, i.e., at 0.5 cm from the cathode, level ($n=2$) seems to be a factor of 5 more populated than level ($n=4$), and at 1 cm, the ratio of ($n=2$) to ($n=4$) is even equal to 6. This is in reasonable agreement with the statistical weights of both levels, which would predict a factor of 5 difference in population density (i.e., $g=5$ for $n=2$ and $g=1$ for $n=4$).

The other two $4s,4s'$ levels ($n=3,5$) are not metastable but they can decay towards the ground state by emission of radiation; this additional loss (depopulation) process explains the somewhat lower population density of these levels. Except close to the cathode, the level populations seem to decrease in the order: $(n=2)>(n=4)>(n=3)>(n=5)$. In Ref. 31 the level populations of the $4s,4s'$ levels were calculated and measured for a range of currents and pressures, and the level populations were found to decrease in the same order $4s[3/2]_2$ $(n=2)>4s'[1/2]_0$ $(n=4)>4s[3/2]_1$ $(n=3)>4s'[1/2]_1$ $(n=5)$, which is, at least qualitatively, in good agreement with our results. A slightly different order was, however, found in Ref. 23 for a magnetron discharge. At high currents ($\sim$1 A) it appeared that $4s[3/2]_2$ $(n=2)>4s[3/2]_1$ $(n=3)>4s'[1/2]_0$ $(n=4)>4s'[1/2]_1$ $(n=5)$, but at lower currents the $4s'[1/2]_0$ level population became comparable to the $4s[3/2]_1$ population and at 0.1 A (100 mA, i.e., the lowest current presented in their article), the $4s'[1/2]_0$ level ($n=4$) was again more populated than the $4s[3/2]_1$ level ($n=3$), which corresponds well with our findings at a still lower current of 2 mA.

The $4s,4s'$ nonmetastable levels exhibit a somewhat different density profile compared to the $4s,4s'$ metastable levels. Indeed, the density is zero at the walls (because the levels are all deexcited at the walls), but increases to a pronounced maximum immediately adjacent to the cathode wall, because the lifetime of these levels is small and diffusion from this position to the walls followed by de-excitation can be neglected with respect to radiative decay. This maximum near the cathode is also caused by fast argon ion and atom impact excitation (which is only important close to the cathode where the ions and atoms can reach high energies) and corresponds to the cathode glow in the glow discharge. Further away from the cathode, the level population decreases almost linearly, but a very small second maximum is observed in the beginning of the NG (the interface between CDS and NG was calculated for the present discharge conditions to be at about 0.15 cm from the cathode[59]).

Similar density profile shapes can be observed in Fig. 3, where the population densities of the $4p,4p'$ levels are illustrated. The profiles are only depicted till $z=1$ cm, since they are negligible further in the cell. The designation of these effective levels, their excitation energy, and statistical weight were presented in Table I. In Ref. 25 different argon atom lines were recorded in a direct current glow discharge, and the optical emission line profiles originating from the lower $4p,4p'$ levels were also characterized by a pronounced maximum in the cathode glow and a small second peak in the beginning of the NG, which is very similar to our population density profiles. Figure 3 shows that the ratio of cathode glow to NG peak decreases slightly with increasing excitation energy of the $4p,4p'$ levels (i.e., the peak in the NG is hardly visible for $n=6$, 7, and 8, whereas it is only a factor 3 smaller than the cathode glow peak for $n=11$). Indeed, the peak near the cathode is caused by fast argon ion and atom impact excitation from the ground state level, whereas the NG peak arises mainly from electron impact excitation from the ground state. Ion and atom impact excitation become only important at rather high ion and atom energies (100–1000 eV and more, which is generally higher than the mean energies of the argon ions and atoms at the present glow discharge conditions, e.g., less than 100 eV) whereas electron impact excitation is already significant at lower energies. It is clear that for highly excited levels more energy is required to produce the same amount of excitation compared to lower levels, and hence that ion and atom impact excitation become less efficient (since the argon ion and atom energies are not high enough for efficient excitation) compared to electron impact excitation. This effect can also be observed in the optical emission profiles recorded in Ref. 25: optical emission lines originating from the lower $4p,4p'$ levels have a distinct dominant peak in the cathode glow, whereas this peak decreases gradually and becomes even

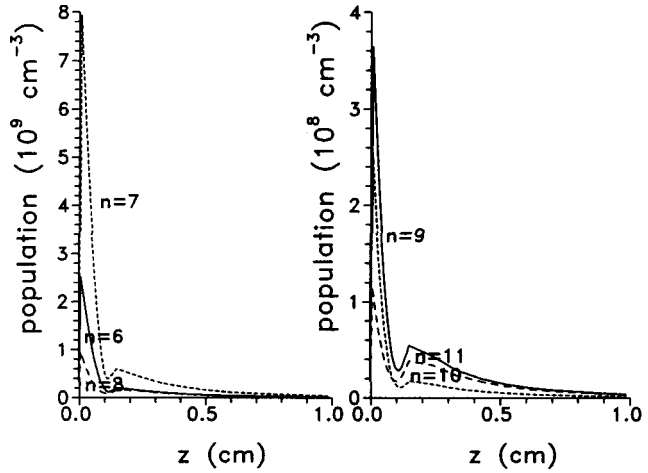

FIG. 3. Calculated level population profiles of the $4p,4p'$ levels, at 1000 V, 1 Torr, and 2 mA. Left part: $n=6$: $4p[1/2]_1$; $n=7$: $4p[3/2]_{1,2}+4p[5/2]_{2,3}$; $n=8$: $4p'[3/2]_{1,2}$. Right part: $n=9$: $4p'[1/2]_1$; $n=10$: $4p[1/2]_0$; $n=11$: $4p'[1/2]_0$.

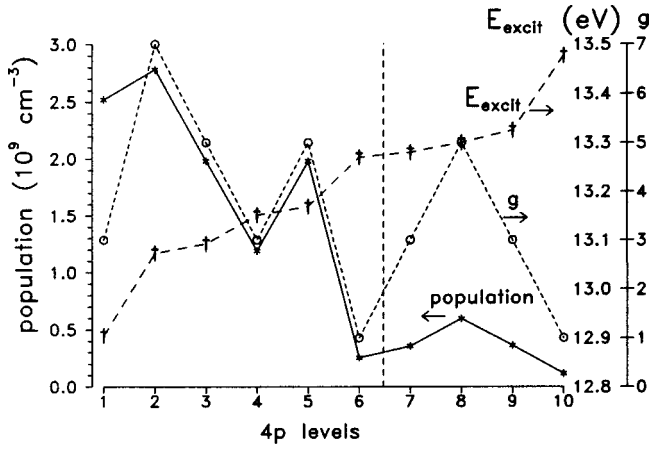

FIG. 4. Calculated level populations at the maxima of their profiles (i.e., adjacent to the cathode) for the individual $4p,4p'$ levels, at 1000 V, 1 Torr, and 2 mA (left axis), as well as their excitation energies and statistical weights (right axes). The numbers on the x axis represent the following $4p,4p'$ levels: $1=4p[1/2]_1$; $2=4p[5/2]_3$; $3=4p[5/2]_2$; $4=4p[3/2]_1$; $5=4p[3/2]_2$; $6=4p[1/2]_0$; $7=4p'[3/2]_1$; $8=4p'[3/2]_2$; $9=4p'[1/2]_1$; $10=4p'[1/2]_0$.

comparable to the NG peak for emission lines arising from the higher $4p,4p'$ levels.

The population densities depicted in Fig. 3 correspond to the effective $4p,4p'$ levels (i.e., various individual levels combined into one effective level according to their excitation energy and core quantum number) and they do not exactly represent the individual $4p,4p'$ level populations. For example, effective level $n=6$ consists of only one individual level (i.e., $4p[1/2]_1$), whereas effective level $n=7$ corresponds to four individual levels (i.e., $4p[3/2]_{1,2}$ and $4p[5/2]_{2,3}$), which is manifested in its higher density, shown in Fig. 3. We have subdivided again the populations of effective levels into the individual levels, based on the statistical weights, and the resulting populations of the individual levels at the maxima of the profiles (i.e., adjacent to the cathode) for all $4p,4p'$ levels are presented in Fig. 4. In the same figure, also the statistical weights and excitation energies of the various $4p,4p'$ levels are indicated. As expected, there is a clear correlation between the level populations and the statistical weights. The trend with respect to the excitation energy (i.e., decreasing population at increasing excitation energy) is only weak, because in fact, the excitation energy varies only a few percent from the lowest to the highest $4p$ level. It is only significant for the lowest $4p$ level ($n=6$: $4p[1/2]_1$), which lies indeed clearly below the other $4p,4p'$ levels (see Fig. 1). The vertical dashed line on the figure divides the levels into the unprimed (core quantum number=3/2, corresponding to the ionization limit $^2P_{3/2}$ in Ar^+) and primed system (core quantum number=1/2, corresponding to the ionization limit $^2P_{1/2}$ in Ar^+). It can be seen that the level populations of the primed system are generally lower than the level populations of the unprimed system, but the same correlation with the statistical weights is still observed.

Figure 4 shows that the $4p,4p'$ level populations range from 1×10^8 to 3×10^9 cm^{-3}, which is several orders of magnitude lower than the $4s,4s'$ level populations. Indeed, as will be shown later, radiative decay towards lower levels is very important in depopulating the levels. The two $4s,4s'$ metastable levels cannot decay to the ground state by emission of radiation (forbidden transitions) and have therefore a rather high population density. The two other $4s,4s'$ levels can decay radiatively to the ground level, but due to the high number density of these ground state atoms ($\sim10^{16}$ cm^{-3} at 1 Torr), a substantial fraction of the radiation is again absorbed (i.e., radiation trapping, leading again to formation of these levels; see above), and the probability of escape of the emitted radiation is rather low, so that the population densities of the two $4s,4s'$ nonmetastable levels are also still considerable. The $4p,4p'$ levels, however, can decay to the $4s,4s'$ levels by emission of radiation, and since the density of the $4s,4s'$ levels is many orders of magnitude lower than the ground level density, radiation trapping is negligible, and all the emitted radiation escapes and gives rise to the depopulation of the $4p,4p'$ levels, resulting in lower population densities.

Figure 5 illustrates the population density profiles of the $3d,3d'$ and $5s,5s'$ effective levels ($n=12-17$). It can be seen that the ratio of cathode glow peak to NG peak has decreased now (but it is still larger than 1), because the excitation energy is higher for these levels and the efficiency of fast argon ion and atom impact excitation decreases at the typical ion and atom energies encountered at the present glow discharge conditions. The profiles show now also a distinct peak in the beginning of the NG, corresponding to electron impact excitation.

Again, the level populations depicted correspond to the effective levels. Subdivision into the individual $3d,3d'$ and $5s,5s'$ levels was again carried out based on the statistical weights, and the resulting populations (this time at the maximum in the negative glow) are given in Fig. 6. The populations seem again to be strongly correlated with the statistical weights, and depend only weakly on the excitation energy. The shift between the populations and the statistical weight values for the individual $3d$ states in Fig. 6 is a consequence

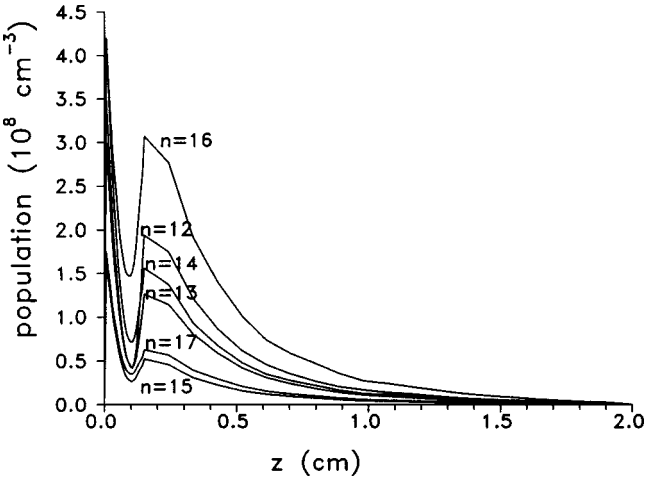

FIG. 5. Calculated level population profiles of the $3d,3d'$ and $5s,5s'$ levels, at 1000 V, 1 Torr, and 2 mA: $n=12$: $3d[1/2]_{0,1}+3d[3/2]_2$; $n=13$: $3d[7/2]_{3,4}$; $n=14$: $3d'[3/2]_2+[5/2]_{2,3}$; $n=15$: $5s'[1/2]_{0,1}$; $n=16$: $3d[3/2]_1+[5/2]_{2,3}+5s[3/2]_{1,2}$; $n=17$: $3d'[3/2]_1$.

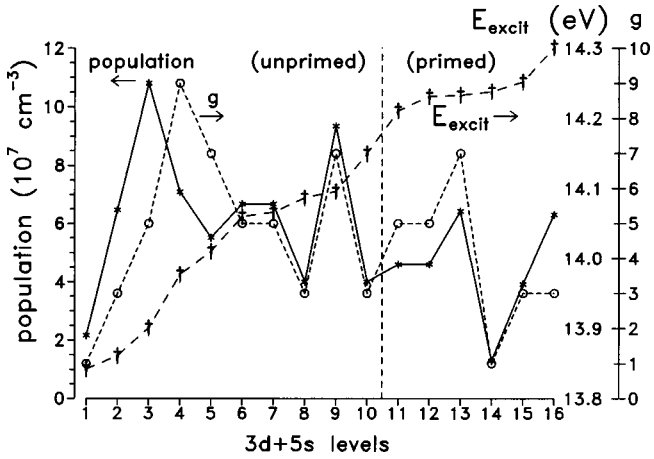

FIG. 6. Calculated level populations in the beginning of the NG for the individual $3d,3d'$ and $5s,5s'$ levels, at 1000 V, 1 Torr, and 2 mA (left axis), as well as their excitation energies and statistical weights (right axes). The numbers on the x axis represent the following $3d,3d',5s,5s'$ levels: 1 $=3d[1/2]_0$; 2 $=3d[1/2]_1$; 3 $=3d[3/2]_2$; 4 $=3d[7/2]_4$; 5 $=3d[7/2]_3$; 6 $=3d[5/2]_2$; 7 $=5s[3/2]_2$; 8 $=5s[3/2]_1$; 9 $=3d[5/2]_3$; 10 $=3d[3/2]_1$; 11 $=3d'[5/2]_2$; 12 $=3d'[3/2]_2$; 13 $=3d'[5/2]_3$; 14 $=5s'[1/2]_0$; 15 $=5s'[1/2]_1$; 16 $=3d'[3/2]_1$.

of the lower cross section for electron impact excitation of the effective level $n=13$ (i.e., $3d[7/2]_{3,4}$) from the ground state in comparison with that for the effective level $n=12$ (i.e., $3d[1/2]_{0,1}+3d[3/2]_2$). The population densities of the $3d,3d'$ and $5s,5s'$ levels vary between 1×10^7 and 1×10^8 cm^{-3} which is clearly lower than the $4p,4p'$ level populations (Fig. 4). However, it should be mentioned that the $4p,4p'$ level populations in Fig. 4 correspond to the pronounced maxima in the cathode glow; the values in the NG are generally a factor of 10 lower (except for $n=11$). Hence, it follows that in the NG the $3d,3d'$ and $5s,5s'$ levels are only slightly lower than the $4p,4p'$ levels. The vertical dashed line in the figure divides again the levels into the unprimed and primed system, like in Fig. 4; it can again be seen that the level populations of the primed system are somewhat lower than the level populations of the unprimed system with the same statistical weights.

The population profiles of the still higher excited levels ($n>17$) show all more or less the same behavior: they are not characterized by a strong peak in the cathode glow anymore, but they reach a maximum at about 0.2 cm from the cathode (in the beginning of the NG). The level populations at the maxima of these profiles are presented in Fig. 7, as a function of the effective level number n. The effective levels $n=18$, 19, 20, and 21 correspond to the $5p,5p'$ and $4d+6s$, $4d'+6s'$ levels, respectively, which are the next excited levels after the $3d,3d'$ and $5s,5s'$ levels (see Table I and Fig. 1), and it is therefore not unexpected that their level populations are still rather high. The levels $n=27$ ($5d+7s$) and $n=33$ ($6d+8s$) are also quite high. Indeed, the transitions from the ground state to these levels are allowed (in contrast to the f and p levels), and the cross sections for electron excitation from the ground level are rather high, yielding a large production and hence high level populations. For the higher levels ($n>21$), it is generally seen that the odd effective level numbers (corresponding to the unprimed system; see Fig. 1) have clearly higher level populations than the even level numbers (which correlate to the primed system). This is mainly attributed to the differences in statistical weights, i.e., the statistical weights of the unprimed (odd) levels are generally two times the values corresponding to the preceding primed (even) levels, as is also illustrated in Fig. 7. However, this is apparently not the only reason because it can be noticed in the figure that the variations in level populations are clearly higher than the statistical weight variations. Another reason is the following. The excited levels are populated, among others, by stepwise excitation from the $4s,4s'$ metastable levels. The excitation from a primed to an unprimed system, and vice versa (i.e., intercombination transition) is of rather low probability, and since the unprimed $4s$ metastable level population ($n=2$) is a factor of 5 to 6 higher than the population of the primed $4s'$ metastable level (except close to the cathode where the ratio is only a factor 1.5), it is indeed to be expected that the higher

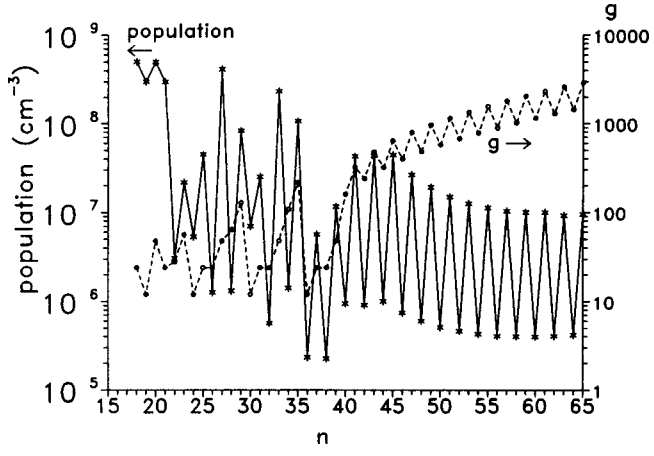

FIG. 7. Calculated level populations at the maxima of their profiles (i.e., in the beginning of the NG) for the higher excited levels ($n>17$; for their designation: see Table I of Ref. 3), at 1000 V, 1 Torr, and 2 mA (left axis), as well as their statistical weights (right axis).

unprimed levels are also more populated than the primed levels. It can also be deduced from Fig. 7 that, in general, the level populations decrease slightly with increasing level number, and hence excitation energy. The trend is not very clear, but when one takes into account that the statistical weights of the levels increase with rising level number (see also Fig. 7, i.e., more individual levels are combined into one effective level; see Table I), the effect will appear somewhat more pronounced.

B. Populating and depopulating processes

Table II lists the calculated relative contributions of the different populating and depopulating processes for the various levels, integrated over the entire (one dimensional) discharge region (i.e., from cathode to anode). For the $4s$ levels ($n=2-5$), excitation from the ground level ($n=1$) by fast argon atom impact, but also by fast argon ion and electron impact, are very important production processes. Besides, production by radiative decay from the $4p$ levels is also of major importance. The latter is in rather good agreement with Ref. 60 where it is concluded that the total cross section for $4s$ metastable level excitation is dominated by cascade contributions. Moreover, stepwise electron excitation, especially from the lowest $4s$ metastable level ($n=2$) to the next $4s$ nonmetastable level ($n=3$), seems also to play a non-negligible role. The remaining production processes incorporated in our model appear to be negligible, and are, therefore, not included in the table. Concerning the depopulating processes, collisions between two atoms in the metastable levels and Penning ionization of sputtered atoms seem the dominant loss processes for the $4s$ metastable levels ($n=2$ and 4). Moreover, electron impact excitation from the lowest $4s$ metastable level ($n=2$), primarily to the next $4s$ nonmetastable level ($n=3$), is also a rather important loss mechanism. The same is true for the other $4s'$ metastable level ($n=4$), which is also converted to the highest $4s'$ nonmetastable level ($n=5$) by electron excitation. Furthermore, electron excitation from the metastable levels to the $4p$ levels is also responsible for a few %. Two- and three-body collisions with argon ground state atoms are of minor importance, as well as electron, ion, and atom excitation to higher levels and electron impact ionization from the metastable levels. As far as the nonmetastable $4s$ levels ($n=3,5$) are concerned, radiative decay to the ground level is clearly the dominant loss processes, and all the other processes can be considered negligible.

Table II presents also the relative contributions of the different populating and depopulating processes for two $4p$ levels, i.e., a low ($n=7$) and a high level ($n=11$). It follows again that fast argon atom impact excitation, and also fast argon ion and electron impact excitation from the ground level, are very important production processes, as is also radiative decay from higher excited levels, especially from the $3d$ and $5s$ levels. To a lesser extent, also stepwise electron, fast argon ion and atom impact excitation from the $4s$ levels (especially from $n=2$) play a role in populating the $4p$ levels. For the loss processes, radiative decay to the four $4s$ levels are by far the dominant depopulating processes (radiative decay to the ground level is not allowed based on the selection rules).

We compared our findings that stepwise excitation from the $4s$ metastable levels is more important for the lower $4p$ levels (i.e., a contribution of a few % of the total production) than for the higher $4p$ levels (i.e., virtually zero contribution) with the results of Ref. 61. The two argon atomic spectral lines studied in that work are the 811.5 nm line and the 750.4 nm line. The first line corresponds to the transition from $4p[5/2]_3$ ($n=7$; hence a lower $4p$ level) to $4s[3/2]_2$ ($n=2$), whereas the second line connects $4p'[1/2]_0$ ($n=11$; hence the highest $4p$ level) with $4s'[1/2]_3$ ($n=5$). It was shown in Ref. 61 that stepwise excitation from the $4s$ metastable levels is almost an order of magnitude faster for the production of the 811.5 nm line (i.e., for populating the $4p[5/2]_3$ level; $n=7$) than for the production of the 750.4 nm line (i.e., for populating the $4p'[1/2]_0$ level; $n=11$), which is indeed in satisfactory qualitative agreement with our findings.

The $3d$ and $5s$ levels are primarily populated by electron impact excitation from the ground state, and for a few percent, by electron stepwise excitation from the $4s$ levels, as is illustrated in Table II for $n=16$. Since the excitation energies of the levels are becoming higher, fast argon ion and atom impact excitation from the ground state become less important, although their contribution is still far from negligible. Radiative decay from higher excited levels, especially from the $5p$ levels, is also quite significant. By far the dominant depopulating process is radiative decay to the $4p$ levels; radiative decay to the $4s$ levels is not allowed, and decay to the ground state has a lower probability, because a substantial fraction of the emitted radiation will again be absorbed by the large population of ground state atoms (radiation trapping), which leads to repopulation of the excited level.

The $5p$, $4d$, and $6s$ levels, which are represented in Table II by levels 18 and 20, resp., are mainly populated by electron impact excitation from the ground state and radiative decay from higher excited levels. Fast argon ion and atom impact excitation from the ground state play still some role, in spite of the relatively high excitation energies of these levels. Moreover, excitation and de-excitation from other excited levels, due to collisions with electrons or thermal argon atoms have also a small contribution, because these higher excited levels are lying close to each other, making transitions from one level to another more probable. Radiative decay transitions to the lower levels are the dominant depopulating processes: the $5p$ levels decay primarily to the $3d$ and $5s$ levels, whereas the $4d$ and $6s$ levels decay about 50/50 to the $4p$ and $5p$ levels. Again, excitation to higher and de-excitation to lower levels due to collisions with thermal argon atoms and electrons are of some importance.

Finally, the relative contributions of the populating and depopulating processes for one of the higher excited levels, i.e., the $12s',p',d',f'\ldots$ levels ($n=50$), are presented in Table II. It can be seen that electron impact excitation from lower levels (not particularly the ground state level, but rather the excited levels, hence stepwise excitation) and de-excitation from higher levels are the dominant populating

TABLE II. Calculated relative contributions (in %) of the populating and depopulating processes, integrated over the entire discharge region, at 1000 V, 1 Torr, and 2 mA, for some selected levels (for their designations: see Table I).

Level n	Populating processes (%)	Depopulating processes (%)
2	elec.excit.from ground state ($n=1$): 1.68	metastastable-metastable collisions: 47.4
($4s[3/2]_2$)	elec.deexcit.from higher $4s$: 0.84	Penning ionization of sputtered atoms: 33.3
	ion excit.from ground state ($n=1$): 10.6	elec.excit.to higher $4s$: 12.7
(4: similar)	fast atom excit.from ground state ($n=1$): 44.6	elec.excit.to $4p$: 3.24
	rad.decay from $4p$($n=6-11$): 41.7	
3	elec.excit.from ground state ($n=1$): 4.29	rad.decay to ground state ($n=1$): 98.7
($4s[3/2]_1$)	elec.excit.from lower $4s$: 5.81	
	elec.deexcit.from higher $4s$: 0.34	
(5: similar)	ion excit.from ground state ($n=1$): 12.6	
	fast atom excit.from ground state ($n=1$): 53.0	
	rad.decay from $4p$($n=6-11$): 23.6	
7	elec.excit.from ground state ($n=1$): 8.89	rad.decay to $4s[3/2]_2$($n=2$): 64.6
(low $4p$)	elec.excit.from $4s$($n=2-5$): 2.44	rad.decay to $4s[3/2]_1$($n=3$): 28.7
	ion excit.from ground state ($n=1$): 13.2	rad.decay to $4s'[1/2]_0$($n=4$): 1.13
	ion excit.from $4s$($n=2-5$): 0.3	rad.decay to $4s'[1/2]_1$($n=5$): 5.53
	fast atom excit.from ground state ($n=1$): 46.4	
	fast atom excit.from $4s$($n=2-5$): 1.29	
	rad.decay from $3d$, $5s$($n=12-17$): 21.6	
	rad.decay from higher levels: 5.55	
11	elec.excit.from ground state ($n=1$): 51.4	rad.decay to $4s[3/2]_2$($n=2$): 0
(high $4p$)	elec.excit.from $4s$($n=2-5$): 0.11	rad.decay to $4s[3/2]_1$($n=3$): 0.51
	ion excit.from ground state ($n=1$): 3.49	rad.decay to $4s'[1/2]_0$($n=4$): 0
	ion excit.from $4s$($n=2-5$): 0.1	rad.decay to $4s'[1/2]_1$($n=5$): 96.5
	fast atom excit.from ground state ($n=1$): 10.2	
	fast atom excit.from $4s$($n=2-5$): 0.43	
	rad.decay from $3d$,$5s$($n=12-17$): 32.1	
	rad.decay from higher levels: 2.11	
16	elec.excit.from ground state ($n=1$): 46.8	rad.decay to ground state ($n=1$): 0.1
($3d$,$5s$)	elec.excit.from $4s$($n=2-5$): 3.16	rad.decay to $4p$($n=6-11$): 98.5
	ion excit.from ground state ($n=1$): 1.08	
	fast atom excit.from ground state ($n=1$): 3.17	
	rad.decay from $5p$($n=18,19$): 38.5	
	rad.decay from higher levels: 6.57	
18	elec.excit.from ground state ($n=1$): 49.6	rad.decay to $4s$($n=2-5$): 14.9
($5p$)	ion excit.from ground state ($n=1$): 1.39	rad.decay to $3d$,$5s$($n=12-17$): 81.3
	fast atom excit.from ground state ($n=1$): 4.07	elec.exc.to higher+de-exc.to lower: 2.9
	elec.exc.from lower+de-exc.from higher: 1.78	therm.at.exc.to higher+de-exc.to lower: 0.86
	therm.at.exc.from lower+de-exc.from higher: 0.63	
	rad.decay from $4d$,$6s$($n=20,21$): 37.5	
	rad.decay from higher levels: 4.9	
$n=20$	elec.excit.from ground state ($n=1$): 75.0	rad.decay to ground state ($n=1$): 0.11
($4d$,$6s$)	ion excit.from ground state ($n=1$): 3.2	rad.decay to $4p$($n=6-11$): 47.5
	fast atom excit.from ground state ($n=1$): 9.36	rad.decay to $5p$($n=18,19$): 46.4
	elec.exc.from lower+de-exc.from higher: 3.0	elec.exc.to higher+de-exc.to lower: 5.1
	therm.at.exc.from lower+de-exc.from higher: 1.1	therm.at.exc.to higher+de-exc.to lower: 0.85
	rad.decay from higher levels: 8.32	
$n=50$	elec.excit.from lower+de-excit.from higher: 71.7	rad.decay to lower levels: 0.22
(high	therm.at.exc.from lower+de-exc.from higher: 23.6	elec.exc.to higher+de-exc.to lower: 70.3
level)	fast ion exc.from lower+de-exc.from higher: 1.62	therm.at.exc.to higher+de-exc.to lower: 21.3
	fast at.exc.from lower+de-exc.from higher: 2.71	fast argon ion exc.to higher+de-exc.to lower: 0.82
	rad.decay from higher levels: 0.05	fast argon at.exc.to higher+de-exc.to lower: 6.82

processes. Excitation and de-excitation between closely lying levels, due to collisions with thermal argon atoms or fast argon ions or atoms, are, however, becoming increasingly important for the higher levels. Indeed, the highly excited levels are lying close to each other and the argon atom and ion energies are sufficient to yield conversions from one level to another. Radiative decay from higher excited levels becomes of lower importance, not only because the number of higher-lying levels decreases when the effective level number of the level under consideration increases, but also because radiative transitions start playing a minor role for the higher excited levels (see below). As far as the loss processes

are concerned, radiative decay to the lower levels becomes less important for the higher excited levels (although the number of lower lying levels increases). These levels seem, however, to be primarily depopulated by electron and thermal and fast argon atom and argon ion impact excitation and de-excitation to other levels.

V. CONCLUSION

A CR model for an argon glow discharge is described, taking into account 65 effective levels of argon atoms and all processes that can in theory play a role, i.e., radiative decay, electron, fast argon ion, fast argon atom and thermal argon atom impact ionization, excitation and de-excitation between all the levels, electron-ion radiative recombination and electron-ion three-body recombination where the third body is an electron, fast argon ion or atom, or a thermal argon atom. Some additional processes are incorporated for the two $4s$ metastable levels, i.e., Penning ionization of sputtered atoms, two- and three-body collisions with argon ground state atoms, collisions between two metastable levels, and diffusion and subsequent de-excitation at the walls. The cross sections and reaction coefficients for all these processes are discussed.

The results (i.e., level population profiles for the various levels, and the relative contributions of populating and depopulating processes) are presented at discharge conditions of 1000 V, 1 Torr, and 2 mA. The level populations of the $4s,4s'$ metastable levels are somewhat higher than the corresponding $4s,4s'$ nonmetastable level populations. Moreover, the $4s,4s'$ levels are much more populated than the $4p,4p'$ and higher levels. In general, the level populations of the excited levels are strongly correlated to their statistical weights and decrease slightly with increasing excitation energy. Concerning the different populating and depopulating processes, radiative decay seems to be dominant as production and loss process for the low-lying levels, although electron, fast argon ion, and especially fast argon atom impact excitation from the ground state are also important production processes. The higher excited levels are primarily populated and depopulated by electron, fast argon ion, and fast and thermal argon atom excitation and de-excitation between the various levels.

ACKNOWLEDGMENTS

A. Bogaerts is financially supported by the Flemish Fund for Scientific Research (FWO). A. Bogaerts and R. Gijbels also acknowledge financial support from the Federal Services for Scientific, Technical and Cultural Affairs (DWTC/SSTC) of the Prime Minister's Office through IUAP-IV (Conv. P4/10). This work was also sponsored by a NATO-Collaborative Research Grant, Project No. HTECH CRG970529. Finally, the authors would like to express their gratitude to J. Loureiro and J. van der Mullen for interesting and helpful discussions.

[1] R. K. Marcus, *Glow Discharge Spectroscopies* (Plenum, New York, 1993).
[2] R. Payling, D. Jones, and A. Bengtson, *Glow Discharge Optical Emission Spectrometry* (Wiley, Chichester, 1997).
[3] A. Bogaerts, M. van Straaten, and R. Gijbels, Spectrochim. Acta B **50**, 179 (1995).
[4] A. Bogaerts, R. Gijbels, and W. J. Goedheer, J. Appl. Phys. **78**, 2233 (1995).
[5] A. Bogaerts and R. Gijbels, J. Appl. Phys. **78**, 6427 (1995).
[6] A. Bogaerts and R. Gijbels, Phys. Rev. A **52**, 3743 (1995).
[7] A. Bogaerts, R. Gijbels, and W. J. Goedheer, Anal. Chem. **68**, 2296 (1996).
[8] A. Bogaerts, M. van Straaten, and R. Gijbels, J. Appl. Phys. **77**, 1868 (1995).
[9] A. Bogaerts and R. Gijbels, J. Appl. Phys. **79**, 1279 (1996).
[10] A. Bogaerts and R. Gijbels, Anal. Chem. **68**, 2676 (1996).
[11] D. R. Bates, A. E. Kingston, and R. W. P. McWhirter, Proc. R. Soc. London, Ser. A **267**, 297 (1962).
[12] D. R. Bates, A. E. Kingston, and R. W. P. McWhirter, Proc. R. Soc. London, Ser. A **270**, 155 (1962).
[13] R. W. P. McWhirter and A. G. Hearn, Proc. Phys. Soc. London **82**, 641 (1963).
[14] H. R. Griem, Phys. Rev. **131**, 1170 (1963).
[15] H. W. Drawin and F. Emard, Physica C **85**, 333 (1977).
[16] T. Fujimoto, J. Phys. Soc. Jpn. **47**, 265 (1979).
[17] A. M. Gomés, J. Phys. D **16**, 357 (1983).
[18] B. van der Sijde, J. J. A. M. van der Mullen, and D. C. Schram, Beitr. Plasmaphys. **24**, 447 (1984).
[19] T. Hasegawa and H. Haraguchi, Spectrochim. Acta B **40**, 1067 (1985).
[20] D. A. Benoy, J. A. M. van der Mullen, B. van der Sijde, and D. C. Schram, J. Quant. Spectrosc. Radiat. Transf. **46**, 195 (1991).
[21] J. Vlcek, J. Phys. D **22**, 623 (1989).
[22] L. L. Alves, G. Gousset, and C. M. Ferreira, J. Phys. D **25**, 1713 (1992).
[23] F. Guimaraes and J. Bretagne, Plasma Sources Sci. Technol. **2**, 127 (1993).
[24] A. V. Phelps and B. M. Jelenkovic, Phys. Rev. A **38**, 2975 (1988).
[25] K. Rozsa, A. Gallagher, and Z. Donko, Phys. Rev. E **52**, 913 (1995).
[26] D. A. Scott and A. V. Phelps, Phys. Rev. A **43**, 3043 (1991).
[27] C. E. Moore, Natl. Stand. Ref. Data Ser. (U.S., Natl. Bur. Stand.) (1971).
[28] T. Holstein, Phys. Rev. **83**, 1159 (1951).
[29] P. J. Walsh, Phys. Rev. **116**, 511 (1959).
[30] J. W. Mills and G. M. Hieftje, Spectrochim. Acta B **39**, 859 (1984).
[31] C. M. Ferreira, J. Loureiro, and A. Ricard, J. Appl. Phys. **57**, 82 (1984).
[32] J. Vlcek and V. Pelikan, J. Phys. D **22**, 632 (1989).
[33] N. Thonnard and G. S. Hurst, Phys. Rev. A **5**, 1110 (1972).
[34] R. C. Michaelson and A. L. Smith, J. Chem. Phys. **61**, 2566 (1974).
[35] J. H. Kolts and D. W. Setser, J. Chem. Phys. **68**, 4848 (1978).
[36] M. Cacciatore, M. Capitelli, and H. W. Drawin, Physica C **84**, 267 (1976).
[37] A. Bogaerts and R. Gijbels, Fresenius J. Anal. Chem. **359**, 331 (1997).
[38] Y. Weng and M. J. Kushner, Phys. Rev. A **42**, 6192 (1990).
[39] S. Hashiguchi, IEEE Trans. Plasma Sci. **19**, 297 (1991).
[40] J. Bretagne, G. Delouya, J. Godart, and V. Puech, J. Phys. D **14**, 1225 (1981).
[41] R. J. Carman, J. Phys. D **22**, 55 (1989).
[42] D. Rapp and P. Englander-Golden, J. Chem. Phys. **43**, 1464 (1965).
[43] H. A. Hyman, Phys. Rev. A **20**, 855 (1979).
[44] H. W. Drawin, Fontenay-aux-Roses Report, EUR-CEA-FC-383, 1967 (unpublished).
[45] A. Kimura, H. Kobayashi, M. Nishida and P. Valentin, J. Quant. Spectrosc. Radiat. Transf. **34**, 189 (1985).
[46] J. Bretagne, J. Godart, and V. Puech, J. Phys. D **15**, 2205 (1982).
[47] F. J. de Heer, R. H. J. Jansen, and W. van der Kaay, J. Phys. B **12**, 979 (1979).
[48] A. Bogaerts and R. Gijbels, Plasma Phys. Rep. (in press).
[49] A. V. Phelps, J. Appl. Phys. **76**, 747 (1994).
[50] H. W. Drawin and F. Emard, Phys. Lett. A **43**, 333 (1973).
[51] A. V. Phelps, J. Phys. Chem. Ref. Data **20**, 557 (1991).
[52] V. Kempter, G. Riecke, F. Veith, and L. Zehnle, J. Phys. B **9**, 3081 (1976).
[53] K. Tachibana, Phys. Rev. A **34**, 1007 (1986).
[54] W. L. Wiese, J. W. Brault, K. Danzmann, V. Helbig, and M. Kock, Phys. Rev. A **39**, 2461 (1989).
[55] L. A. Riseberg, W. F. Parks, and L. D. Schearer, Phys. Rev. A **8**, 1962 (1973).

[56] S. Inaba, T. Goto, and S. Hattori, J. Phys. Soc. Jpn. **52**, 1164 (1983).
[57] A. Bogaerts, R. D. Guenard, B. W. Smith, J. D. Winefordner, W. W. Harrison, and R. Gijbels, Spectrochim. Acta B **52**, 219 (1997).
[58] B. K. McMillin and M. R. Zachariah, J. Appl. Phys. **77**, 5538 (1995).
[59] A. Bogaerts and R. Gijbels, J. Anal. At. Spectrom. **12**, 751 (1997).
[60] N. J. Mason and W. R. Newell, J. Phys. B **20**, 1357 (1987).
[61] Z. Lj. Petrovic, S. Bzenic, J. Jovanovic, and S. Djurovic, J. Phys. D **28**, 2287 (1995).